Preliminary Orbit Determination Using the Transit of Satellites in Front of Space-Based Illumination Sources

Daniel M. Dombrowski
Masters Student Air Force Institute of Technology, Department of Aeronautics and Astronautics
Robert A. Bettinger
Faculty Air Force Institute of Technology, Department of Aeronautics and Astronautics

ABSTRACT

A novel method of preliminary satellite orbit determination is presented utilizing a union of the techniques used in astronomical occultation analysis, short arc orbit determination techniques integral to asteroid orbit determination, and satellite optical tracking. Departing from the convention of employing ground- and/or space-based radar to obtain angle and position data for near-Earth orbit determination, such information is instead obtained by using a combination of ground or space-based visual light sensor and a space-based mirror. In this new method, the space-based mirror reflects light towards the Earth and the resultant illumination disk is observed for the transit of satellites or other resident space objects (RSO). The sensor observes the passing shadow of the satellite or RSO and directly computes the relative position of the object casting the shadow to the space-based mirror.

Traditionally, the problem of orbit determination based on azimuth and elevation data has been handled using classical angles-only orbit determination techniques, such as Laplace's or Gauss's Method. The proposed system creates a novel orbit determination technique using the known geometry of the space-based reflector, illumination disk optical data, and a linearized orbit model. The accuracy of this novel method will be compared with traditional orbit determination techniques for accuracy and to determine applicability for different orbital regimes. This method would meld the advances made in the astronomy field with that of near-Earth orbit determination and could provide particular benefit to spacecraft lost after initial orbit insertion.

1. INTRODUCTION

Large space-based reflectors have been researched extensively in the past for use in reflecting solar energy back to Earth for a variety of uses including illumination of large urban areas, emergency operations, farming, and enhancing photosynthesis [1][2] . Should a reasonably large nadir pointing solar reflector be placed into orbit, it would act as a point light source. This would cause anything that passes through its cone of reflected light to cast a shadow onto the Earth with a negligible penumbra creating shadows with well-defined edges. This fact allows for a novel reverse occultation problem. Historically, stellar occultations have been used to determine the shape parameters of objects as far as the Kuiper Belt [3]. In this novel occultation problem, the shadow from a resident space object (RSO) is observed and a translational orbit model is derived using the inertial position and velocity vectors. One of the benefits of this method is that all three components of the inertial position vector can be calculated simultaneously, as opposed to angular data and rates as is common in optical tracking techniques or range and range rates as is common in satellite laser ranging [4].

In further detail, the satellite or RSO passes through the illumination cone provided by the reflected light from the space-based mirror. The resultant shadow is then observed. Using basic trigonometry, a relative position vector from the space-based mirror to the transiting object is then created utilizing the position of the centroid of the observed shadow and trigonometric data. This relative position vector in the space-based mirror's body reference frame is then converted to the Earth-centered inertial frame. The relative position vector is then added to the position vector of the space-based mirror to result in the position vector of the RSO. Using a linearized model and a high frequency optical sensor the velocity vector of the spacecraft or RSO can then be derived. Having computed an Earth-based inertial position and velocity vector, the RSO's classic two body orbit is then fully determined and can be propagated both forward and backward in time.

An astrodynamicaly accurate software simulation has been developed to create a video upon which to test this technique. This program takes inputs of the space-based mirror's and RSO's classical orbital elements (COEs) and optical sensor parameters and outputs a video simulation and the propagated position data of the space-based mirror.

These outputs are then fed into a second software program to analyze the video using the novel orbit determination technique developed herein and outputs the COEs of the RSO. The results from this software will then be compared to show the efficacy of this novel orbit determination technique. Circumstances under which this novel method may prove particularly advantageous will be discussed.

The method proposed is deterministic in nature. In order to increase the efficacy of this model, the research in occultation solutions and short arc orbit determination must be melded. In recent years, short arc orbit determination methods have seen significant research in the realm of asteroid orbit determination as well as satellite optical tracking [5]. This research could prove invaluable to this technique. For the scope of this paper, however, the deterministic model will be applied and tested to gain initial quantitative data for this novel initial orbit determination (IOD) method. It has been shown that accurate orbit determination can be performed with dense observational data (several hundred observations per pass) [6]. This is ideally suited to this IOD method. Using either modest frame rate cameras or luminosity sensors hundreds of dense observations can be gathered quickly.

2. INITIAL ORBIT DETERMINATION ALGORITHM

The first step in this novel IOD method is to observe the shadow cast by a RSO travelling through the illumination cone provided by the space-based illumination source. The illumination cone will be assumed to be pointing nadir for the purposes of this paper. This cone will have an opening angle equal to the solar angular diameter at Earth hereon referred to as α, which is approximately constant throughout Earth's orbit with a value of 0.0093 radians [2]. This illumination cone will intersect with the surface of the Earth, assumed to be flat over the length of the resultant illuminated circle on the Earth. Any object traveling through the illumination disk will then cast a shadow onto the Earth. The projection of this shadow on the Earth will be an ellipse throughout the transit, or circular should the RSO pass directly underneath the reflector. Fig. 1 provides a two-dimensional representation of the transit.

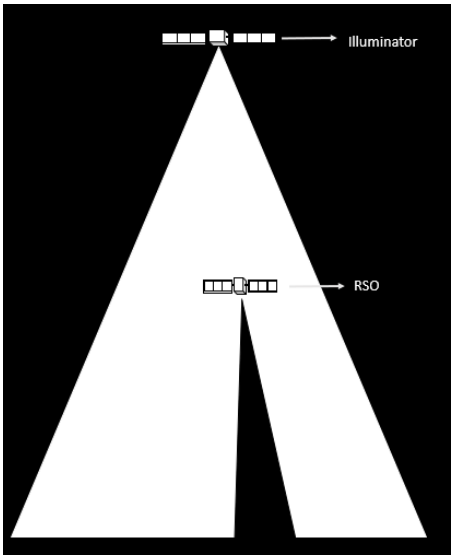

Fig. 1. Two-Dimensional Transit Geometry

In the following analysis two orbital frames of reference will be utilized. The first is the Earth-centered inertial (ECI) frame defined as $\hat{e_1}$ pointing towards the vernal equinox, $\hat{e_2}$ pointing perpendicularly eastward, and $\hat{e_3}$ completing the right-handed coordinate frame. The second is an reflector satellite fixed local-vertical-local-horizontal (LVLH) frame defined as $\hat{e_1}$ pointing in the negative radial direction, $\hat{e_3}$ in the negative orbit normal direction, and $\hat{e_2}$ completes the right-handed coordinate frame. The shadow ellipse cast onto the Earth must be measured to determine the semiminor and semimajor axes of the ellipse (b and a, respectively), the position of the centroid in the second and third dimension of the LVLH frame (the first dimension, essentially depth, is unknown at this point). These quantities can be determined by use of a space-based sensor or ground based luminosity detector system.

In order to find the relative position of the RSO with respect to the illuminator, the altitude of the RSO above the Earth is first calculated using the geometry of the shadow ellipse. When the transit geometry is observed perpendicular to the shadow ellipse minor axis in two dimensions the shadow appears to form an isosceles triangle as shown in Fig. 2.

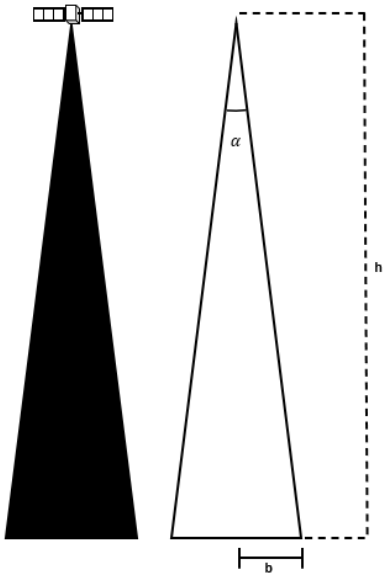

Fig. 2. Two-Dimensional Minor Axis View of Shadow Geometry

Using this view, the altitude of the RSO (h) can clearly be determined from the trigonometric relationship shown in Eqn. (1).

$$h = \frac{b}{\tan(\alpha)} \tag{1}$$

The RSO's altitude can then be used in order to calculate the position of the RSO with respect to the shadow ellipse's centroid (at the intersection of sides ρ and a in Fig. 3).

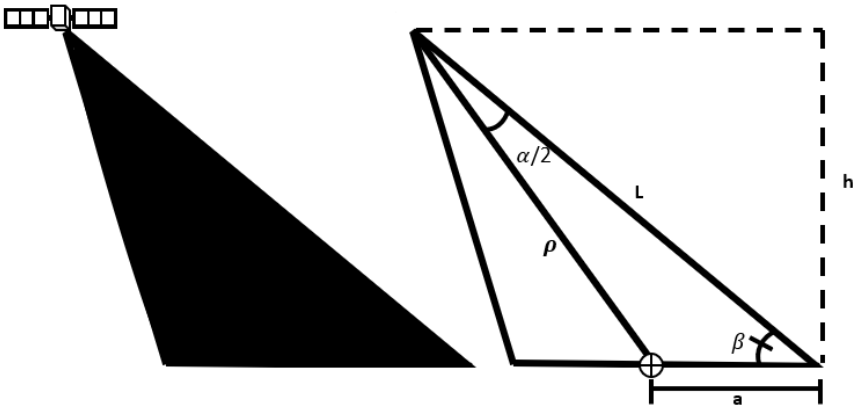

Fig. 3. 2D Major Axis View of Shadow Geometry

If the position of the centroid of the shadow is known, then the distance from the RSO to the shadow centroid ρ must be calculated in order to fully define the three-dimensional position of the RSO. The values of L and β determined through knowledge of h found from Eqn. (1), the constant α, and the semimajor axis length. This geometry problem then reduces through defining two equations and two unknowns which can then be solved simultaneously as shown in Eqns. (2) and (3) below. Eqn. (2)is a simple trigonometric identity for the right triangle with h as a side and L as the hypotenuse and Eqn. (3) is an application of the Law of Sines on the triangle ρ-a-L.

$$cos(\beta - 90^0) = \frac{h}{L} \tag{2}$$

$$\frac{a}{sin(\alpha)} = \frac{L}{sin(180^0 - \alpha - \beta)} \tag{3}$$

With quantities L and β known, ρ can be calculated through the use of the Law of Cosines as shown in Eqn. (4).

$$\rho = \sqrt{a^2 + L^2 - 2aL\cos(\beta)} \tag{4}$$

The relative position of the RSO with respect to the illuminator is then shown in Eqn. (4), with $C_{\odot}(2)$, $C_{\odot}(3)$ being the shadow center position in the LVLH frame $\hat{e_2}$ and $\hat{e_3}$ directions, respectively.

$$[\bar{R}_{rel}]^{LVLH} = [R_{illuminator} - (R_{\oplus} + h), \quad C_{\odot}(2) - \rho * \hat{R}_{C_{\odot}}(2), \quad C_{\odot}(3) - \rho * \hat{R}_{C_{\odot}}(3)]^T \tag{5}$$

A series of rotations can then be used to convert this vector from the LVLH frame into the ECI frame. With this relative position vector in the ECI frame, simple vector addition can be used to ultimately calculate the position of the RSO in inertial space as shown in Fig. 3 and Eqn. (6). This technique can be used to calculate the inertial position vector of the RSO at each data point.

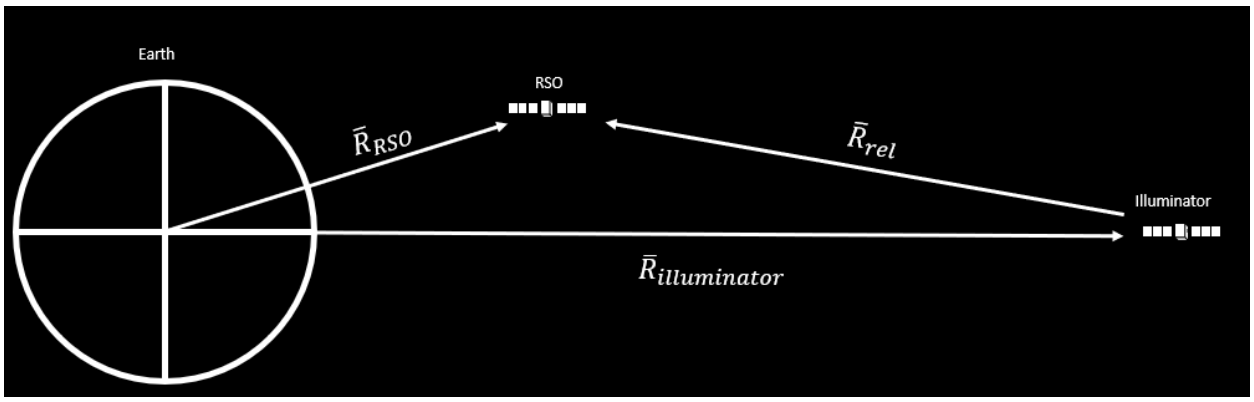

Fig. 4. Vector Geometry Representation

$$\bar{R}_{RSO} = \bar{R}_{illuminator} + \bar{R}_{Rrel} \tag{6}$$

Three methods of velocity calculation are used in conjunction with this technique to test for efficacy within the low Earth orbit (LEO) regime: namely linearization, circularization, and the Herrick-Gibbs method. Knowing both a current and a past inertial position vector for the RSO and assuming a sufficiently short time step, the linear velocity vector can be approximated as shown in Eqn. (7).

$$\bar{V}_{RSO}(n) = \frac{\bar{R}_{RSO}(n) - \bar{R}_{RSO}(n-1)}{\Delta t} \tag{7}$$

Most objects in LEO have very low eccentricities due to their proximity to Earth, as a high eccentricity at this point would force the RSO into atmospheric reentry. This provides a second method, similar to linearization, but instead assuming circular travel within the time step. A change in the inertial position vector ($\widehat{\Delta R}$) is calculated as shown in Eqn. (8). The average position vector is then used to calculate a scalar circular velocity which is then projected onto the change in $\widehat{\Delta R}$ as given by Eqn. (9).

$$\widehat{\Delta R} = \frac{\bar{R}_{RSO}(n) - \bar{R}_{RSO}(n-1)}{\|\bar{R}_{RSO}(n) - \bar{R}_{RSO}(n-1)\|} \tag{8}$$

$$\bar{V}_{RSO}(n) = \sqrt{\frac{\mu}{\frac{\bar{R}_{RSO}(n) - \bar{R}_{RSO}(n-1)}{2}}} \cdot \widehat{\Delta R} \tag{9}$$

The final method is the Herrick-Gibbs method. For sake of brevity, a thorough discussion of this well-known technique will be left to other authors [4]. Implementation of this technique will be performed through use of Vallado's Herrick-Gibbs algorithm which supplemented his text *Fundamentals of Astrodynamics and Applications* [11]. Comparisons between the three methods will be analyzed to determine how a rough approximation (derivative and circular techniques) compares to Herrick-Gibbs more mathematically rigorous technique.

3. SOFTWARE IMPLEMENTATION OF IOD TECHNIQUE

MATLAB (version 2020b) was used to realize an initial program based off the IOD algorithm that receives a video file and position data for the reflector and generates COEs for the RSO to be tested for accuracy. In order to simplify the program, it is assumed that the reflector and RSO follow two body motion, the reflector and the observational instrument are co-located in a geostationary orbit, and the size of the RSO is negligible compared to the shadow size. First, the program uses the input COEs of the reflector satellite and RSO and a fourth-order Runge-Kutta integrator to numerically propagate both orbits for the duration of time specified within the input. The relative position of the position of the RSO with respect to the reflector is then calculated in a similar fashion as discussed before, shown in Eqn. (10).

$$\bar{R}_{Rrel} = \bar{R}_{RSO} - \bar{R}_{illuminator} \tag{10}$$

Next, a binary image of the illumination disk is created to represent an optical instrument aboard the reflector satellite and aligned with the $\hat{e_2}$ and $\hat{e_3}$ axis of the LVLH reference frame. The image is square with 400 km ground distance per side and each pixel represents 100 m. A base image is used to create an illuminated circle, as expressed by Eqn. (11), using a flat-Earth approximation over the picture size.

$$r = alt_{geo} * \tan\left(\frac{\alpha}{2}\right) = 35788.1km * \tan(.00465) = 166.4km \tag{11}$$

In order to animate the RSO's shadow, the relative position vector is rotated into the LVLH frame via Eqn. (12), where l is the reflector satellites true longitude.

$$[\bar{R}_{rel}]^{LVLH} = \begin{bmatrix} \cos(\pi) & 0 & \sin(\pi) \\ 0 & 1 & 0 \\ -\sin(\pi) & 0 & \cos(\pi) \end{bmatrix} \begin{bmatrix} \cos(l) & -\sin(l) & 0 \\ \sin(l) & \cos(l) & 0 \\ 0 & 0 & 1 \end{bmatrix} [\bar{R}_{rel}]^{IJK} \tag{12}$$

The equation of a three-dimensional half cone centered at the RSO and whose central axis is aligned with the relative position unit vector is then set equal to the plane of the Earth directly under the reflector. The intersection of the three-dimensional plane and cone yields an ellipse along the plane. This plane runs perpendicular to the $\hat{e_1}$ LVLH axis such that when this ellipse is filled in, it represents the objects shadow. This binary image is finally converted into an eight-bit integer value to be saved as a standard .avi video frame; the results of which are shown in below in Fig. 5.

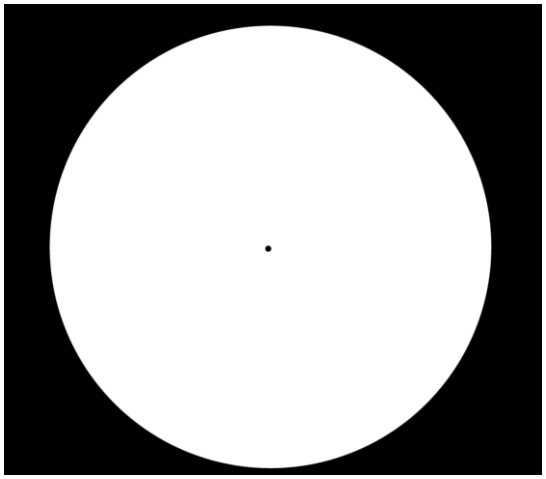

Fig. 5. Example Binary Video Frame

For the next frame, a new relative position vector is calculated and the process of re-animating the RSO's shadow is repeated once per frame for the requested duration of the video and upon completion of this loop the video file is saved as well as the position data from the reflector satellite for use in the orbit determination program. For the purposes of initial testing, a frame rate of 30 frames per second was used.

Having read in the video file, the orbit determination program must gather geometric information from the image. For this task, the video frame is sent to a computer vision subprogram. The image is first converted into a greyscale image. Next, Otsu's thresholding algorithm is then applied to determine a threshold value which is used to convert the greyscale image into binary [7]. This binary image is then flipped, such that any shadows pixels in the image are converted to a one value for detection. All one-valued shapes in the image are then examined for their size parameters. Any shapes that do not fit expected size parameters, in the case of our situation the size of a LEO RSO's shadow, will be filled in. This leaves an image with only the desired shadows present, and this image and the number of objects detected therein are then sent back to the main IOD program. With the video creation software creating a binary image, the computer vision subprogram was tested against a true color image taken by the NASA's Cassini spacecraft. The image (courtesy of NASA's Jet Propulsion Laboratory) shows Io and its shadow overlaid on Jupiter's surface [8]. Fig. 6 below provides a visual depiction of the computer vision process on this image.

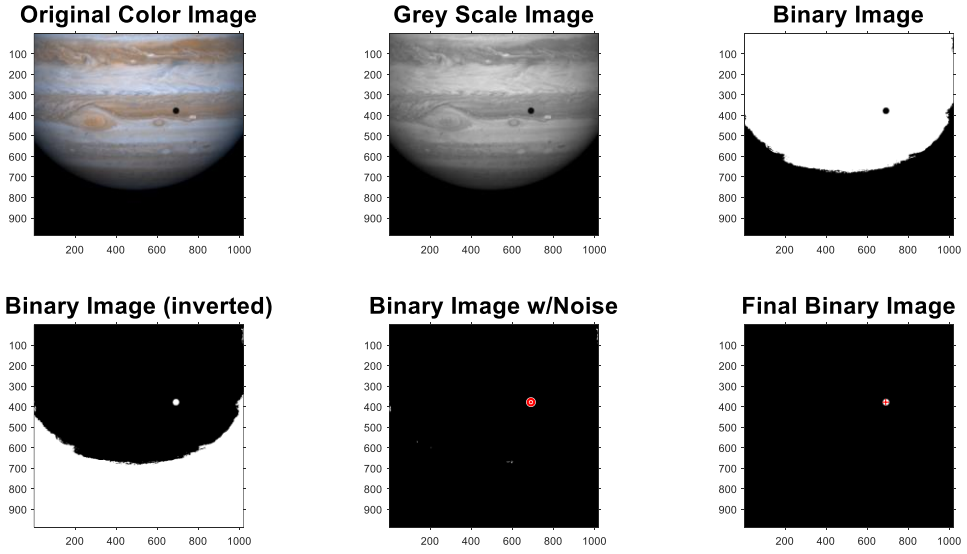

Fig. 6. Example Binary Video Frame

If the computer vision subprogram does not detect any shadows, then the program continues directly to the next frame. If shadows are indeed detected, then the program measures the shadow's semiminor and semiminor axis lengths, and centroid locations. Using this information, it develops a relative position vector in the LVLH frame as described by Eqns. (1)-(5), previously.

In preliminary testing, significant noise was found in the $\hat{e_1}$ component of the relative position vector in the LVLH frame as shown in Fig. 6. This was due to errors in determining the semimajor and semiminor axis lengths. The $\hat{e_2}$ and $\hat{e_3}$ components experienced no such noise, since their values are dominated by the shadow centroid position terms, $C_{\odot}(2)$ and $C_{\odot}(3)$ respectively. In order to negate the effect of the noise on the $\hat{e_1}$ component, a moving mean filter is implemented with a sliding window length equal to the framerate. A moving mean filter averages the input values (x) within a finite window (N) as shown in Eqn. (13) [9][10].

$$x(n) = \frac{x(n) + x(n-1)\ldots + x(n-\frac{N}{2}) + x(n+1)\ldots + x(n+\frac{N}{2})}{N} \tag{13}$$

As illustrated by Fig. 7, the blue line indicating the filtered $\hat{e_1}$ component of the relative position vector in the LVLH frame has far smaller amplitude oscillations than the unfiltered data in red.

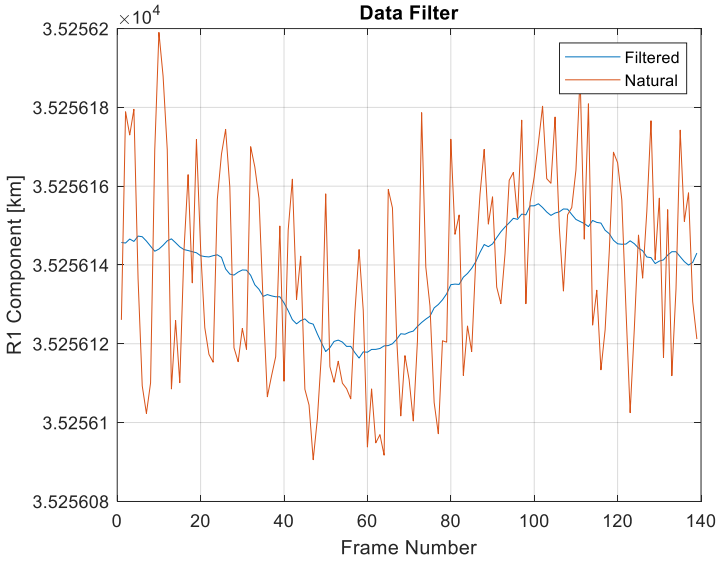

Fig. 7. Filtered $\hat{e_1}$ Relative Position Vector in the LVLH Frame

Rotations about the second and third axes are then used to convert the relative position vector from the LVLH frame into the IJK frame as shown in Eqn. (14).

$$[\bar{R}_{rel}]^{IJK} = \begin{bmatrix} \cos(-l) & -\sin(-l) & 0 \\ \sin(-l) & \cos(-l) & 0 \\ 0 & 0 & 1 \end{bmatrix} \begin{bmatrix} \cos(-\pi) & 0 & \sin(-\pi) \\ 0 & 1 & 0 \\ -\sin(-\pi) & 0 & \cos(-\pi) \end{bmatrix} [\bar{R}_{rel}]^{LVLH} \tag{14}$$

This vector is then added to the inertial position vector of the reflector satellite to determine the inertial position vector of the RSO as described by Eqn. (6) previously.

After calculating the inertial position vector as detailed above, inertial velocities can be calculated as described by Eqn. (7) - Eqn. (9) previously. It is of note that the linearized and circularized methods will only yield $n-1$ full state vectors and the Herrick-Gibbs method will only yield $n-2$ full state vectors since the methods require initial knowledge of two or three observations respectively.

These inertial position and velocity vectors are then converted into COEs using well known conversion equations [4][11]. While the position and velocity vectors do provide a fully defined orbit, COEs are chosen as the final output due to five of the six of these elements being constant, namely semimajor axis, eccentricity, inclination, right ascension of the ascending node, and argument of perigee. Using this fact, these five COEs can be averaged throughout the entire simulation duration. The sixth COE, true anomaly will be average through one second or equivalently 30 data points. While not a precision technique, as an example the average true anomaly change of a LEO orbit with an altitude of 500 km over one second is only 0.0634 degrees.

$$\Delta\nu = \frac{360^0}{P} * 1\,\text{sec} = 0.0634^0 \tag{15}$$

These final six COEs are then saved as the output of the IOD program and can then be compared to the inputs to the video creation program for analysis.

4. RESULTS

As previously mentioned, testing of this technique assumes the reflector/observer are modeled in a geostationary orbit and in a position coincident with the Vernal Equinox at the epoch time. In order to examine how changing one of the RSO's orbit shape parameters effects the COEs three main trials of 25 tests each were performed, varying the semimajor axis, eccentricity, and inclination. It is important once again to note that this method is deterministic and is being applied to a digital program over a significant course of time and will lend heuristic results. In order for this method to be truly accurate, a more complicated statistical method must be devised.

The semimajor axis was varied from 6878.137 km to 18878.137 km in a circular orbit inclined at 45 degrees. The argument of latitude of the RSO was given as 359.8 degrees and the relative motion simulation was propagated for ten seconds. The results provided are given in terms of the predicted RSO's orbital shape parameters (semimajor axis, eccentricity, and inclination) and the angular position is given in argument of latitude since most of the orbits being tested are circular or near circular and this simplifies the angular position data greatly for initial assessments. The results of these 25 trails are outlined in Fig. 8.

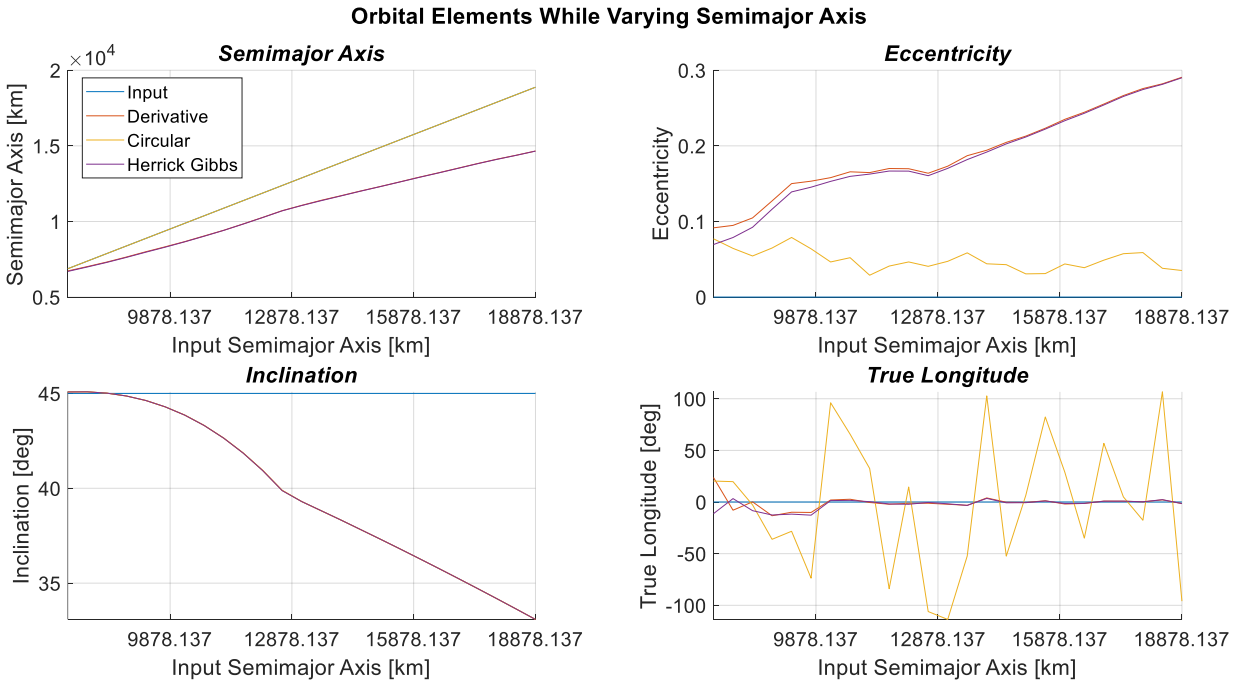

Fig. 8. Orbital Elements while Varying Semimajor Axis

Upon visual inspection, it can be seen that as semimajor axis is increased, the circular method closely tracks this increase while the linear and Herrick-Gibbs method diverge from the input. Eccentricity shows a steady divergence for the linear and Herrick-Gibbs method while the circular method holds approximately constant above the zero valued input. All of the inclination values diverge as the semimajor axis is increased. The derivative and Herrick-Gibbs methods are quite accurate for the initial true longitude value, while the circular approximation had much larger oscillations about the true input value.

The input orbit is circular, so it should come as no surprise that the circular assumption most closely tracks the increasing semimajor axis. The increasing errors in eccentricity for the linear and Herrick-Gibbs methods, as well as inclination for all methods may be attributable to the different rates of relative motion. Lower orbits will cover more relative distance than higher ones within the same 10 second pass, resulting in a greater spread in data points. This variance seems to be necessary to accurately determine the orbital elements. In order to gain a visual sense of these orbits, the input of run number 15 (in blue, altitude of 7,500 km), and the linear (yellow), circular (green), and Herrick-Gibbs (red) approximations are shown in Systems Tool Kit (STK) in Fig. 9.

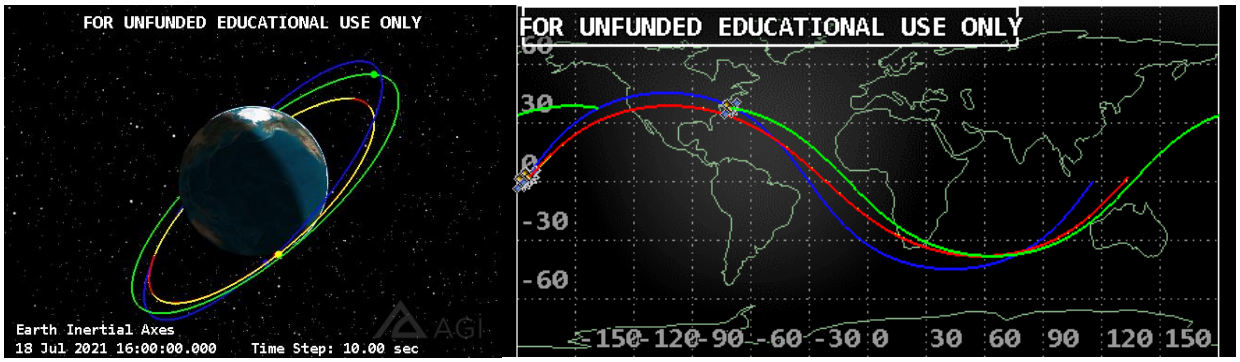

Fig. 9. Three- and Two-Dimensional Representations of Output Orbit Models

The eccentricity was varied from 0.0000001 to 0.1 in an orbit with a semimajor axis of 11378.137 km, an inclination of 45 degrees, right ascension of 0, argument of perigee of 0, and a true anomaly of 359.8 degrees. The results of these 25 trails are given in Fig. 10.

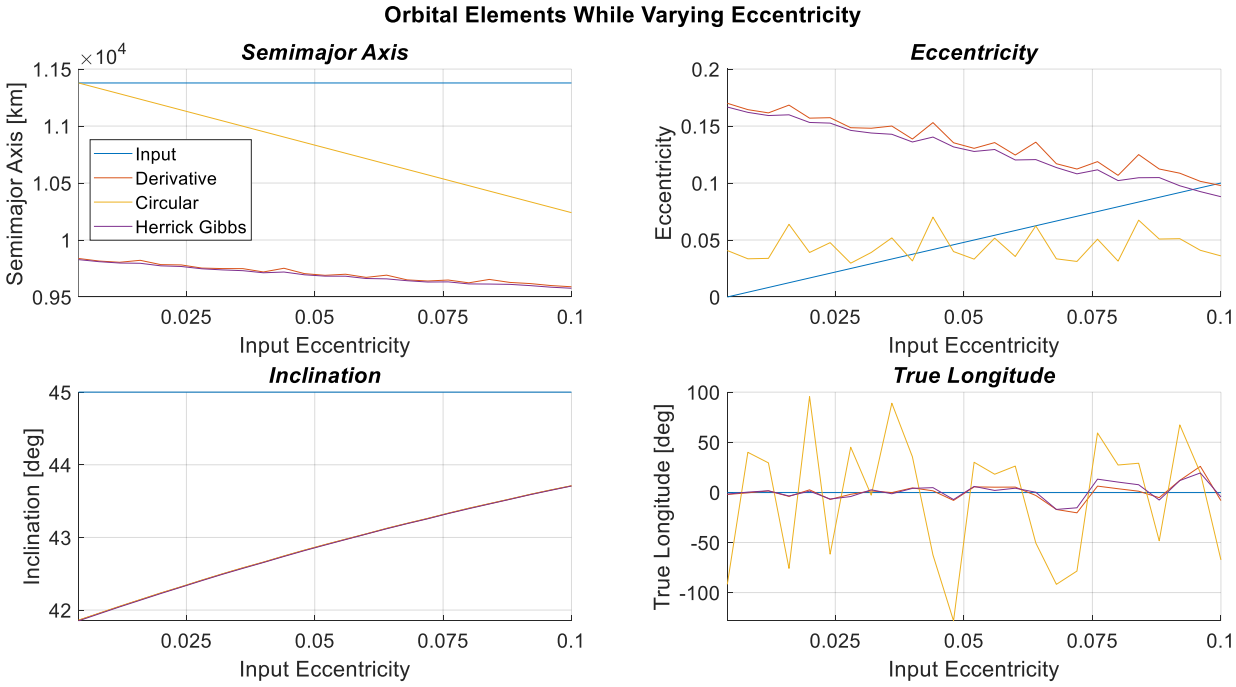

Fig. 10. Orbital Elements while Varying Eccentricity

As expected, Fig. 10 shows that as the eccentricity increases, the circular assumption diverges quickly from the input semimajor axis while the linear and Herrick-Gibbs methods both maintain an underestimate value. It is also expected that the circular assumption maintains an approximately constant value for eccentricity as is observed. The linear and Herrick-Gibbs methods both provide an overestimate of eccentricity, but do converge to the input value at higher values of eccentricity. For near circular orbits (e<0.1) however it seems that the circular approximation provides a good baseline. The error of the inclination value decreases as the eccentricity is increased. Once again, the linear and Herrick-Gibbs approximations tend to have a significantly smaller error in true longitude than the circular approximation.

The underestimation in the RSO's semimajor axis is likely due to the spacecraft's short arc being observed at perigee, and that if it were instead observed at apogee, it would show an overestimate value. This is the main difficulty of developing short arc techniques; it is difficult to make predictions about where the RSO will be half a period later based on a short pass. This could also explain the inclination error decreasing as the eccentricity is increased. At apogee, the RSO will be moving faster providing creating a greater spread in data points for analyzes as discussed previously. Short arc stochastic methods could prove integral to the further development of this technique to resolve this issue.

In order to gain a visual sense of these orbits, the input of run number 15 (in blue, eccentricity of 0.0583), and the linear (yellow), circular (green), and Herrick-Gibbs (red) approximations are depicted in Fig. 11.

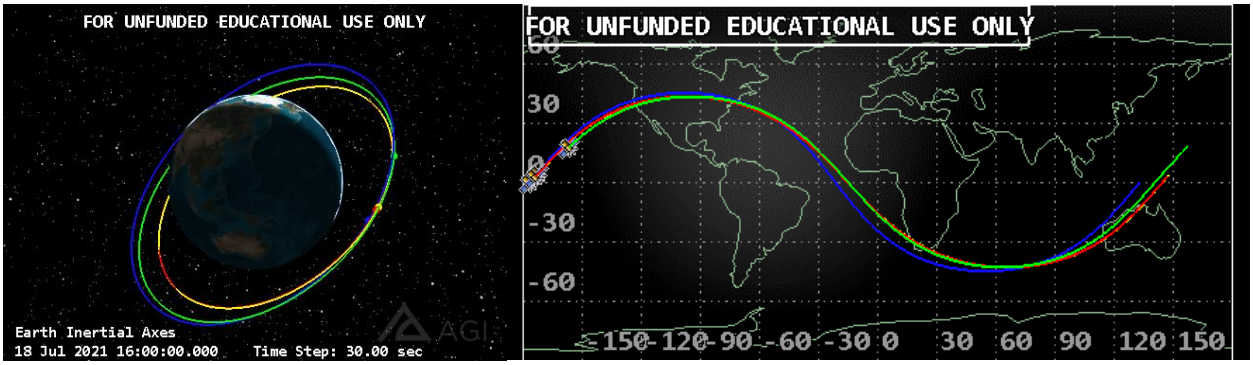

Fig. 11. Three- and Two-Dimensional Representations of Output Orbit Models

Lastly, the inclination was varied from 0 to 180 degrees in a circular orbit with a semimajor axis of 11,378.137km and a true longitude of 359.8 degrees. The results of these 25 trails are given in Fig. 12.

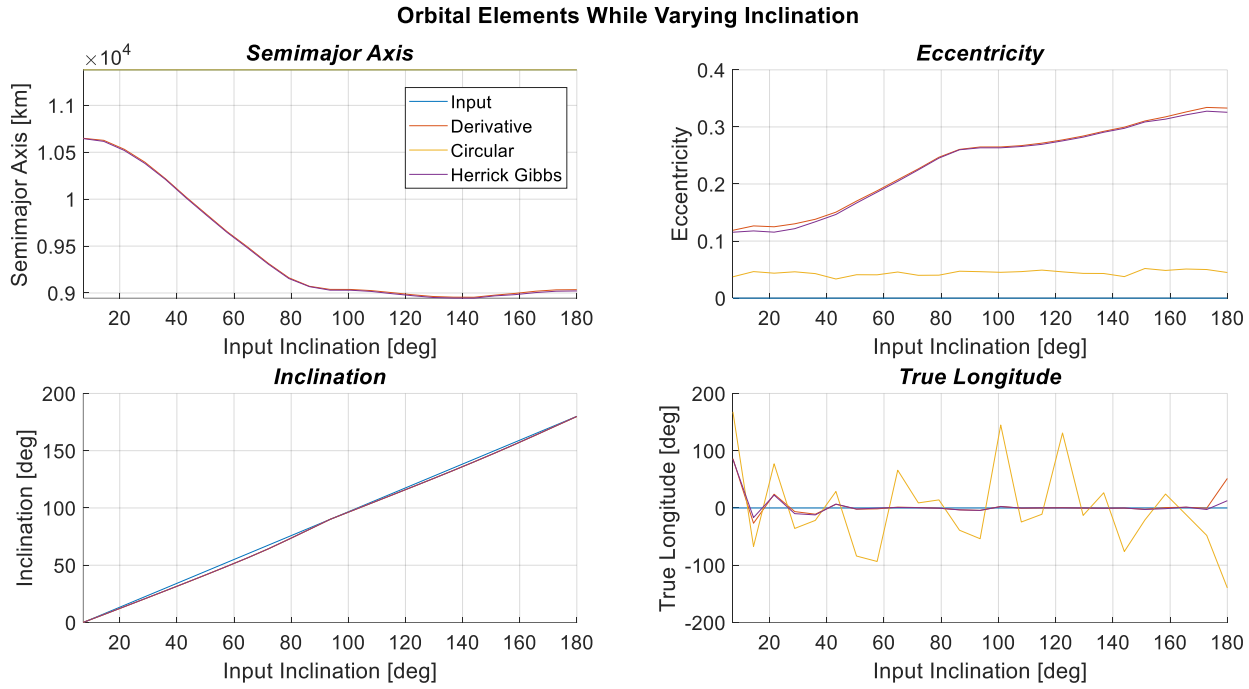

Fig. 12. Orbital Elements while Varying Inclination

Due to the orbit being circular, we once again find that the circular approximation closely matches the semimajor axis, while the linear and Herrick-Gibbs methods provide a diverging underestimate. Similarly, we find a nearly identical plot of the eccentricity as when varying the semimajor axis, with the circular approximation providing a near constant value and the linear and Herrick-Gibbs methods diverging. The inclination plot shows constant accurate tracking. The true longitude again shows the linear and Herrick-Gibbs methods providing a far closer approximation in the majority of cases. In order to gain a visual sense of these orbits, the input of run number 15 (in blue, inclination of 105 degrees), and the linear (yellow), circular (green), and Herrick-Gibbs (red) approximations are shown below in Fig. 13.

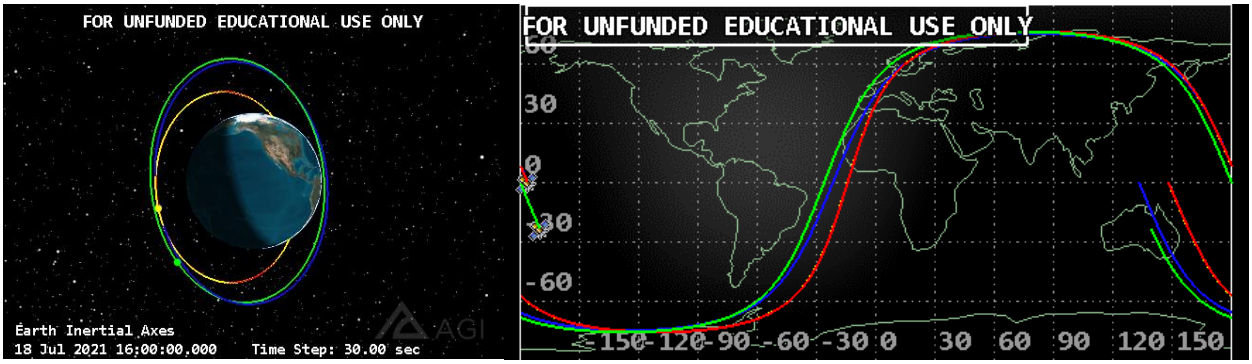

Fig. 13. Three- and Two-Dimensional Representations of Output Orbit Models

5. DISCUSSION

This testing has shown some important heuristic results. It is clear from Figs. 10, 12, and 14 that the most difficult shape parameters to be calculated are the semimajor axis and eccentricity. In testing, eccentricity has proven to be the most difficult to model for low Earth orbits where low values for eccentricity are common. The circular approximation repeatedly provides the most accurate overall orbit shape, however the linear and Herrick-Gibbs methods tend to provide significantly better initial position estimates. These preliminary data points yield confidence that a short arc statistical method can be created that provides results with significantly higher accuracy.

One of the benefits of this method is a large search area to locate an uncooperative RSO. Assuming a geostationary reflector, the radius of the search area for an RSO at 500 km in LEO would be nearly 330 km in diameter. For an uncooperative or tumbling RSO, it can be very difficult to effectively locate it due to changing or masked radar cross sections. Optical observations also require a significant amount of environmental cooperation. There are many ways in which a radar or optical observations can be disrupted, however it is far more difficult for a shadow to be masked. With the growing number of RSOs these benefits avail further development of this method.

In order to increase the efficacy of this IOD technique several further developments are being pursued. First and foremost, a statistical technique must be implemented to utilize the full range of information provided from the dense observation data collected from a pass. Once accomplished, the testing code should be altered to consider various spacecraft cross sectional areas as well as a non-co-located observer and reflector. Upon completion of these updates, the orbits discussed above should be tested. Assuming acceptable results, the technique could then be tested against one of the many LEO catalogs to determine accuracy over a wider range of real-world orbital parameters.

6. SUMMARY

This paper has described the initial progress towards the development of a novel IOD technique based on the transit of a RSO in front of an artificial point light source. This deterministic method melds advances made in the field of astronomy, such as short arc orbit determination and occlusion analysis, with LEO space situational awareness methods. This deterministic method should provide inertial position data accurately to within the precision of available optical instruments. This inertial position data can then be used to create a velocity vector to fully define the translational system.

There are many methods of calculating a velocity vector from the inertial position vector. Three techniques were tested, a linear approximation, a circular approximation, and the Herrick-Gibbs method. In further development of a statistical model, the circular approximation may prove useful for near-circular orbits, while the Herrick-Gibbs technique could yield a better initial estimate over a wider range of orbital eccentricities. Ultimately, this method could prove beneficial in the updating the catalogs containing the ever-increasing number of RSOs in the LEO domain. Should development of space-based solar reflectors continue, this novel method could prove useful in preliminary orbit determination for both cooperative and uncooperative RSOs.

The views expressed are those of the authors and do not reflect the official guidance or position of the United States Government, the Department of Defense or of the United States Air Force.

7. REFERENCES

[1] Canady, J. and J. Allen. “Illumination from space with orbiting solar-reflector spacecraft.” (1982).

[2] Buckingham, Arthur G. and Harold M. Watson. “Basic Concepts of Orbiting Reflectors.” Engineering Notes, July 1968, pp. 851-853.

[3] Buie, Mark W, et al. “Size and Shape Constraints of (486958) Arrokoth from Stellar Occultations.” *The Astronomical Journal*, vol. 159, no. 4, 26 Feb. 2020, doi:10.3847/1538-3881/ab6ced.

[4] Vallado, David A., and Wayne D. McClain. *Fundamentals of Astrodynamics and Applications*. 4th ed., Microcosm Press, 2013.

[5] Choi, Jin, et al. “Characteristics of Orbit Determination with Short-Arc Observation by an Optical Tracking Network, OWL-Net.” *International Journal of Aerospace Engineering*, vol. 2018, 2018, pp. 1–11., doi:10.1155/2018/2837301.

[6] Vallado, David A., and Scott S. Carter. “Accurate Orbit Determination from Short-Arc Dense Observational Data.” *The Journal of the Astronautical Sciences*, vol. 46, no. 2, 1998, pp. 195–213., doi:10.1007/bf03546243.

[7] N. Otsu, "A Threshold Selection Method from Gray-Level Histograms," in *IEEE Transactions on Systems, Man, and Cybernetics*, vol. 9, no. 1, pp. 62-66, Jan. 1979, doi: 10.1109/TSMC.1979.4310076.

[8] “Io in Front of Jupiter.” *NASA Jet Propulsion Laboratory*, NASA, 20 Dec. 2000, www.jpl.nasa.gov/images/io-in-front-of-jupiter.

[9] “How Is a Moving Average Filter Different from an FIR Filter?” *MathWorks Help Center*, MathWorks, www.mathworks.com/help/dsp/ug/how-is-moving-average-filter-different-from-an-fir-filter.html.

[10] “Movmean.” *MathWorks Help Center*, MathWorks, www.mathworks.com/help/matlab/ref/movmean.html.

[11] “Astrodynamics Software by David Vallado.” *CelesTrak*, celestrak.com/software/vallado-sw.php.